Chapter 2
# Anti-Dot Substrates

2.1   Polymer Sphere Lithography Background and Summary

Polymer sphere lithography and, in particular, nanosphere lithography have gained recent attention for a wide range of applications ranging from novel nanofabrication techniques and photonic crystals to superhydrophobic surfaces [8, 63-64]. Most often, because the polymer spheres are typically not treated prior to metal deposition, the resulting patterned film is limited to isolated locations corresponding to the interstices between the template beads [7, 65-66]. With control of the fabrication process, however, the film may form a fully interconnected, yet fully porous network, acquiring what has been termed an 'anti-dot' configuration [67-68]. Specifically, an ordered layer of monodisperse polystyrene (PS) spheres is first applied to the surface of a SOFC electrolyte material; afterwards, the spheres are radially etched in an oxygen plasma, so as to create vias between them. Metal is deposited using a line-of-sight deposition method that enables the still-round PS to serve as a lithographic mask. Upon removal of the polymer template, the desired anti-dot porous structure is obtained. This process is illustrated stepwise in Fig. 2.1.

The periodicity provided by polymer sphere self-assembly is not critically important for SOFC studies; however, sufficient knowledge of microstructural parameters is required, as is high temperature stability. Accordingly, both factors are evaluated below.

Essential to the success of the polymer sphere lithographic technique is achieving a single layer of the polymer spheres across the entirety of the substrate. Several
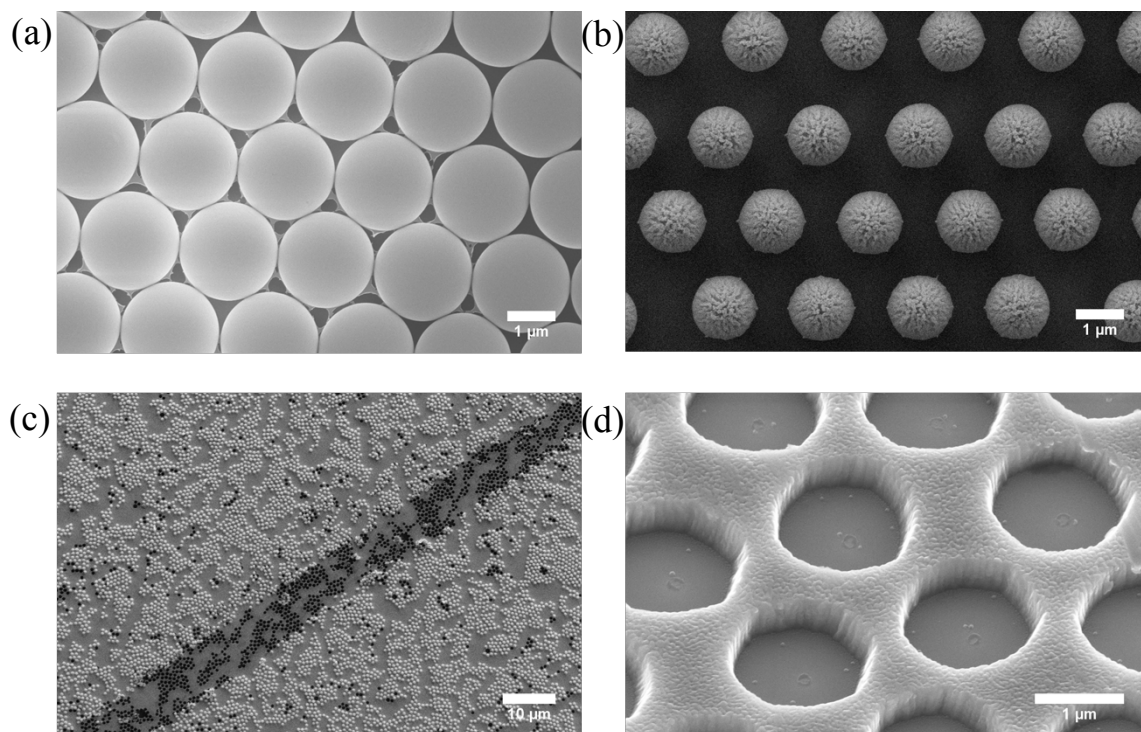
Fig 2.1. The polymer lithography process, all on YSZ: (a) a monolayer of 500 nm polystyrene (PS) spheres; (b) diameter of spheres reduced *via* oxygen plasma etching; (c) metal (Cu) deposited by thermal evaporation; (d) PS spheres removed.

approaches for monolayer deposition have been pursued in the literature, with varying degrees of complexity and experimental constraints. The most common methods are combined sedimentation plus evaporation [69-70]; spin-coating plus evaporation [71]; and controlled evaporation in combination with gradual substrate withdrawal from the solution (dip-coating) [72]. More exotic methods include electrophoretic assembly (suitable only to conducting substrates), and high pressure infusion in combination with ultrasonication [73-75]. While sedimentation, dip-coating, and spin-coating are relatively straightforward methods that produce structures with regularity sufficient for electrocatalysis studies, they suffer from the tendency of the processes to yield regions with multiple layers and others entirely devoid of the polymer spheres. Furthermore,

achieving adequate control of the evaporation step for the former two can require excessive processing times. With the exception of a dip-coating setup encased to provide strict humidity control [72], these methods have difficulty spanning the nanosphere-microsphere range; that is, any given polymer sphere deposition method works with either nanospheres or microspheres, but not both (note: PS spheres less than 1 μm in diameter are herein referred to as nanospheres, whereas spheres greater than 1 μm are referred to as microspheres).

Here, spin coating is employed as a facile means of obtaining the desired monolayers on YSZ and SDC substrates, where a slight variation of the standard spinning approach is necessary for microspheres. Utilization of electronically insulating substrates precludes electrodeposition as a means of subsequent growth of the metallic film, motivating the two-step process pursued here of bead etching and vapor phase metal deposition. For the plasma-etched spheres to serve as effective templates, it is necessary for film growth to be limited to line-of-sight methods that avoid deposition in the void space on the underside of the round beads. Thermal evaporation has been employed in this work for conventional metals (copper, nickel, titanium, titanium/gold, aluminum), whereas electron-beam evaporation has been used for platinum (due to its high melt temperature), with equal effectiveness in all cases. A representative selection of the types of anti-dot electrode structures obtained in this work is presented in Fig. 2.2. The ability to fabricate anti-dot structures from a range of metals on multiple electrolyte materials is essential for ultimate fundamental electrochemical studies.
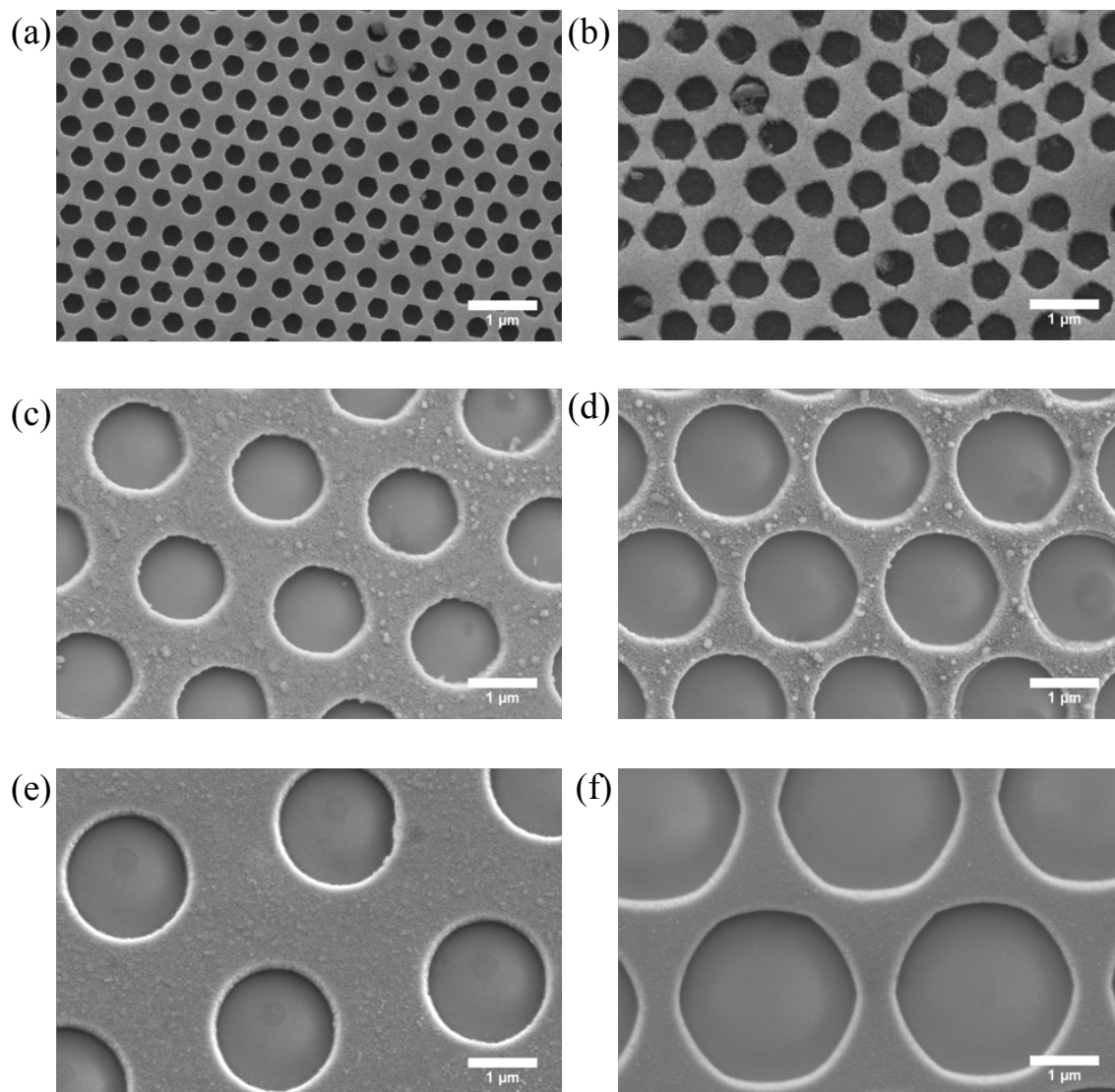
Fig 2.2. Selection of representative copper anti-dot metal films on YSZ showing a range of feature sizes achieved using polymer sphere lithography: (a) 500 nm initial bead size; (b) 790 nm initial bead size; (c) 2 µm initial bead size, heavily etched; (d) 2 µm initial bead size, lightly etched; (e) 3.2 µm initial bead size, heavily etched; and (f) 3.2 µm initial bead size, lightly etched.

2.2   Experimental Details

2.2.1   *Substrate Preparation*

The YSZ substrates (MTI Corporation) used are (100) single-crystals, and the SDC

substrates are epitaxially deposited thin films on single-crystal YSZ via pulsed laser

deposition [32]. For subsequent use for nanosphere deposition, the substrates were

exposed to an oxygen plasma for 5 minutes at 75 W and 250 mTorr (Technics Planar

Etch II) to enhance hydrophilicity. In contrast, as-purchased or as-fabricated substrates

were directly used for microsphere deposition.

2.2.2   *Nanosphere Deposition*

Monolayers were spun using a Laurell, WS-400B-6NPP/LITE spin coater, with a 10 wt%

suspension of PS nanospheres, surface functionalized with carboxyl groups (Bangs

Laboratories, Inc.™). Before spin coating on the substrate, the as-received PS suspension

is sonicated to ensure the beads are homogeneously dispersed. Exactly 35 µL of the

suspension was manually spread over the entire 1 cm x 1 cm substrate before spinning.

The final RPM of the spin coater was 3000 RPM, with varying accelerations depending

on the starting PS diameter. The PS monolayer was radially etched in the same oxygen

plasma system, but at elevated powers (75 – 200 W). In this step, the beads do not move

from their original positions. Typical etching times were anywhere from 5 – 20 minutes.

2.2.3   *Microsphere Deposition*

Non-functionalized PS beads were used for the larger diameters (Thermo Scientific), as

10 wt %. 35 µL of the PS suspension was manually spread over the entire substrate and

spun as before. The spin coater was spun at 4000 RPM. A standard laboratory spray bottle was used to employ the water-wash method, described in detail in Section 2.3.2. If the spin-wash-dry cycle was repeated too many times, immovable multilayers would form. For the 2 μm spheres, the cycle was repeated 3 times; for the 3.2 μm spheres, the cycle was repeated 6 times.

2.2.4 *Metal Deposition*

An in-house constructed thermal evaporation system was used to deposit copper, nickel, titanium, titanium/gold, or aluminum (Alfa Aesar, 99.98+%) at 10^{-5} Torr. Platinum networks were evaporated using an electron beam evaporator (re-manufactured CHA MK-40). The now covered PS beads were removed with an acetone-soaked cotton swab; regardless of the metal deposited, the surface became lustrous after wiping repeatedly, indicating the PS was gone.

2.2.5 *Microstructure Analysis*

Optical photos were taken using a Nikon SMZ1500 stereomicroscope. Electron micrographs were taken on an LEO 1550VP Field Emission SEM. Atomic force microscopy (AFM) images were collected using a Park Systems XE-70 AFM. Image analyses were performed using ImageJ 1.41o freeware. Statistical data pertaining to anti-dot structural features was collected from a series of SEM photos that captured a little over 1% of the total substrate area, constituting 100-400 photos, depending on the magnification used. The number of pores evaluated per sample was 60,000-650,000: the

pore areas were assumed to be perfectly circular, and the diameters were calculated from the individual pore areas.

2.2.6   *High Temperature Stability*

Nickel networks 200 nm thick were brought to 600 ºC under flowing 98.7% H_2 and 1.3% H_2O and held there for 50 hours.

2.3   Results and Discussion

2.3.1   *Nanosphere Lithography Results*

Monolayers of as-purchased, carboxyl-functionalized polystyrene spheres with diameters less than 1 μm (specifically, 500, 680, and 790 nm) were prepared by spin-coating onto a hydrophilic surface (Fig. 2.3), where the optimal spin acceleration, ultimate spin rate, and dwell time were each found to depend on the sphere diameter. Non-functionalized beads displayed insufficient attraction to one another and, consequently, spin-coating resulted in large areas devoid of the template, despite exhaustive attempts at optimizing the spinning conditions. The next step, etching of polystyrene by oxygen plasma treatment, is well-known and was readily applied here [68]. It was observed that short treatments generate contacts between the spheres, presumably as a consequence of softening of the polymer. This undesirable 'necking' was avoided by longer treatments that remove at least ¼ of the original sphere diameter. Finally, in order to ensure the removal of the template without damage to the desired pattern, the film thickness is limited to approximately ½ the diameter of the etched spheres, with the further constraint that a minimum thickness of about 150 nm is required in order to attain acceptable electron transport properties in
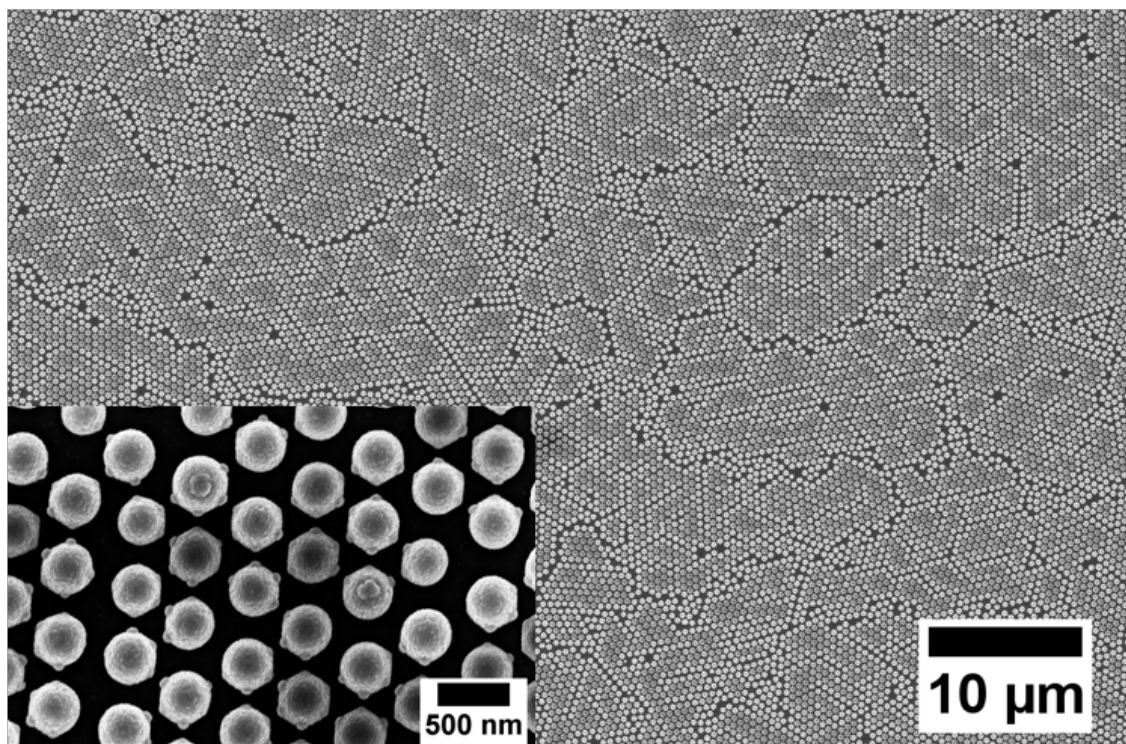
Fig 2.3. SEM images of etched PS beads of 500 nm initial diameter covering large areas of the substrate from a single spin coat step.

the porous film. These considerations preclude fabrication of useful anti-dot electrodes with PS spheres of less than 500 nm in diameter. Fig. 2.4 shows that qualitatively similar coverage is achievable with a variety of different PS sphere diameters.

2.3.2 *Microsphere Lithography Results*

In contrast to the deposition of nanospheres, no set of conditions could be identified for the preparation of a comprehensive monolayer of PS microspheres using a single spin-coating step. Under all accessible spinning conditions, functionalized PS microspheres assembled into irreversible multilayers (see SEM images in Fig. 2.5) that could not be modified for further use due to the line-of-sight nature of the metal deposition step. If metal deposition was pursued regardless of the presence of multilayers, unacceptable
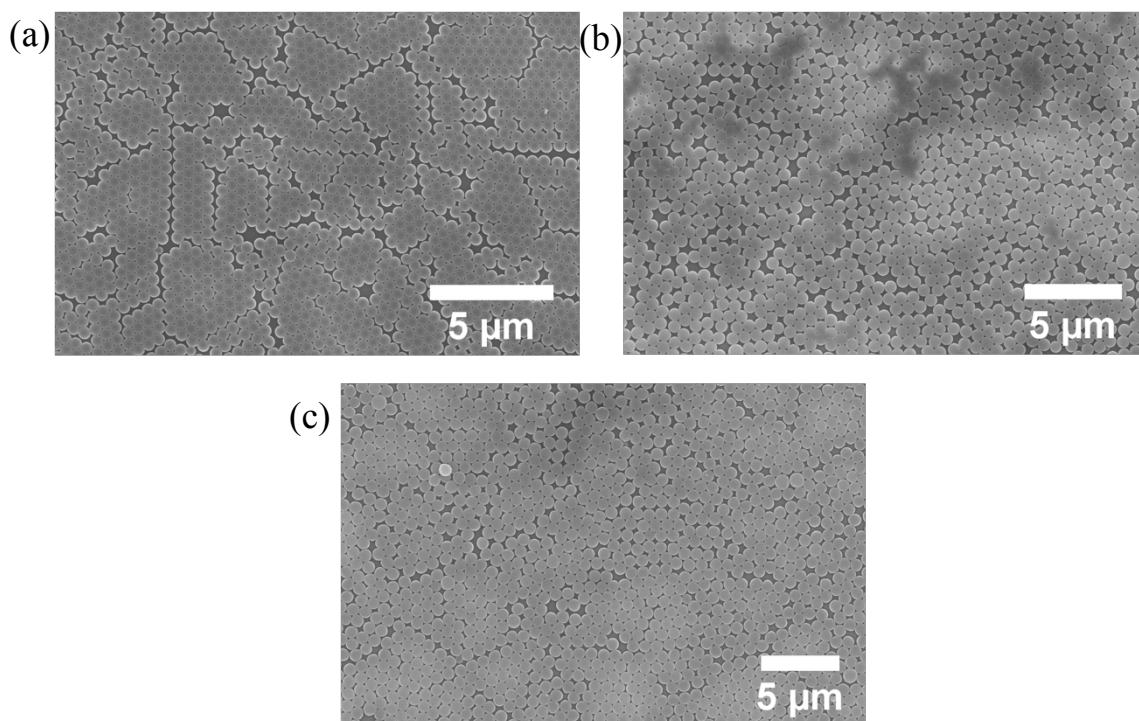
Fig 2.4. Substrate coverage via a single spin-coat for polystyrene nanospheres on YSZ: (a) 500 nm diameter; (b) 680 nm diameter; and (c) 790 nm diameter. Each image contains ~1200 beads.

levels of irregularity in the anti-dot films resulted, as in Fig. 2.5b. In contrast, at high spinning rates, non-functionalized PS microspheres formed monolayers, but with only partial coverage (see Fig. 2.5c), whereas at lower spinning rates multilayer regions emerged (particularly towards the edge of substrate), without elimination of the void areas. A low magnification optical image of such a dilemma is shown in Fig. 2.6, where multilayer regions (white portions) mark the border of the substrate, as well as covering a little less than half of the remaining interior; and void regions (dark areas, more easily seen in Fig. 2.6b) litter the entirety of the interior. The thick multilayer border region is of particular concern, as it can constitute up to 10% of the total substrate.
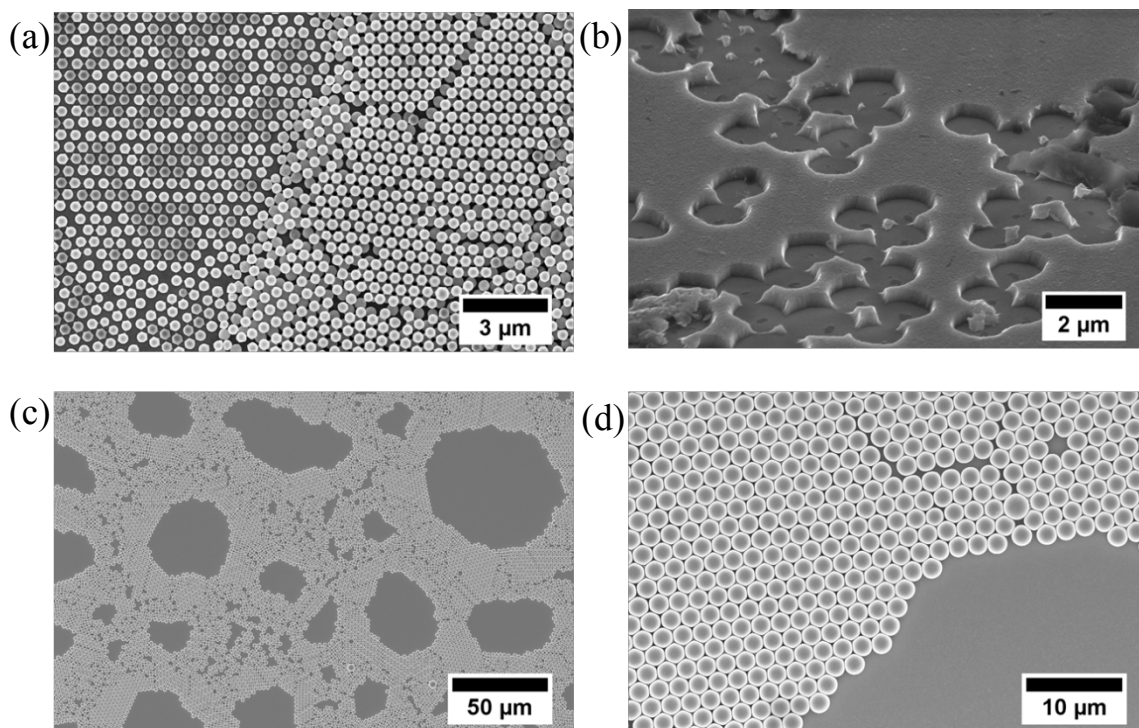
Fig 2.5. (a) Irreversible multilayers formed after a single spin coat of functionalized PS microspheres; (b) the resulting metal film porosity suffers from such multilayers; and (c) and (d) a single spin coat of non-functionalized PS microspheres formed monolayers on most parts of the substrate, but with a significant number of voids.
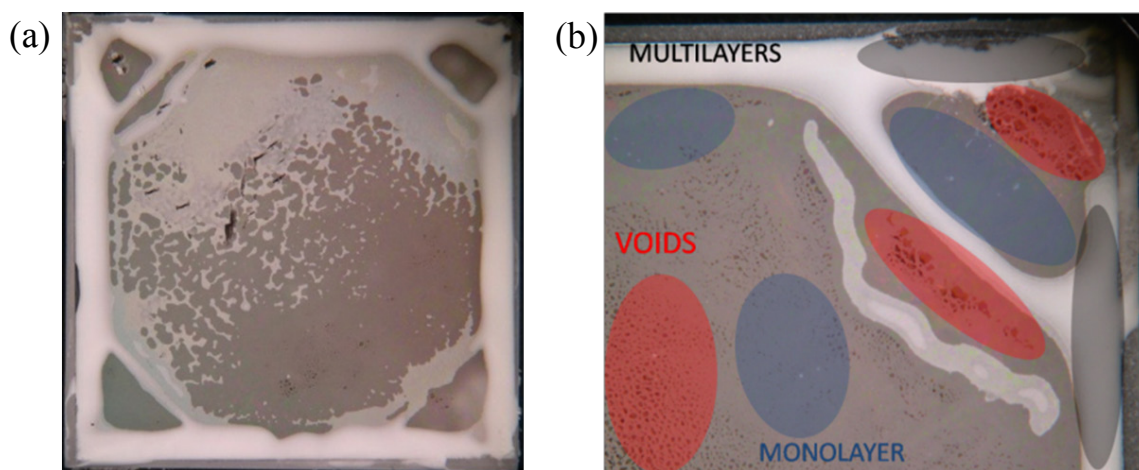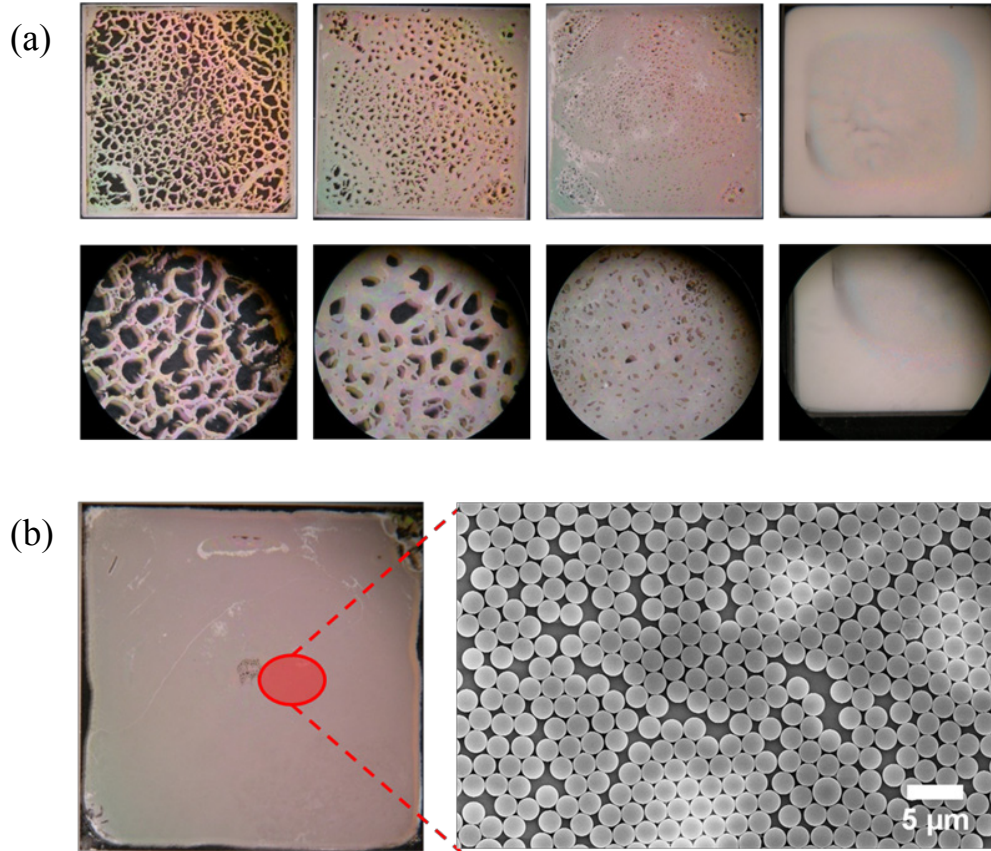

Fig 2.6. Optical photographs of the entire 1 x 1 cm YSZ substrate (a) and a zoomed in view of one corner (b) with a single spin coating of PS microspheres. The white regions are multilayers, the light gray regions are monolayers, and the dark regions are voids.

As an alternative to a single-step monolayer deposition procedure, a process was

developed employing multiple spin-coating steps of the non-functionalized PS beads, depicted in Fig. 2.7. Specifically, a substrate for which the first deposition has yielded a mixture of void regions, monolayer regions and multilayer regions is gently rinsed with water to remove the excess layers in the multilayer regions and the spin-coating is repeated to induce deposition in the void regions. The process is repeated multiple times until the void regions constitute less than about 10% of the substrate area, beyond which multilayer regions cannot be removed by a gentle rinse with water. In a final step, a small amount of the PS suspension is directly applied to the substrate and allowed to dry, eliminating the remaining void regions but with unordered sphere arrangement, as opposed to the relatively periodic arrangement produced by spin coating. For this reason, the spin coating step is repeated as many times as possible before this last step is applied, as disorder in the PS monolayer undoubtedly affects the 3PB/2PB densities. Fig. 2.8 exhibits the most extreme case of utilizing only one spin coat run, resulting in a large portion of the substrate being disordered.

Somewhat fortuitously, the build-up of multilayers causes the otherwise bleakly opaque PS monolayer regions to have a progressively whiter hue—this enables trouble areas to be identified on-the-spot and water-washed more thoroughly, allowing the majority of the void areas to be replaced by an orderly arranged PS monolayer via spin-coating. As will be explicitly shown in Section 2.3.3, the water-wash method produces sufficient coverage and ordering so as to give confidence in the predictability of the theoretical values of 3PB density and 2PB area fraction. As a consequence of these adaptations, microsphere anti-dot substrate preparation is easily repeatable with a high degree of accuracy.

Fig 2.7. (a) The water-wash method utilizes sequential spin coats with water-washing in-between steps. 2 μm beads shown here on a standard 1 x 1 cm YSZ substrate; (b) an optical photograph showing comprehensive monolayer coverage over the entirety of the substrate after the final multilayers are washed off, and a magnified SEM image of a monolayer of 2 μm beads.
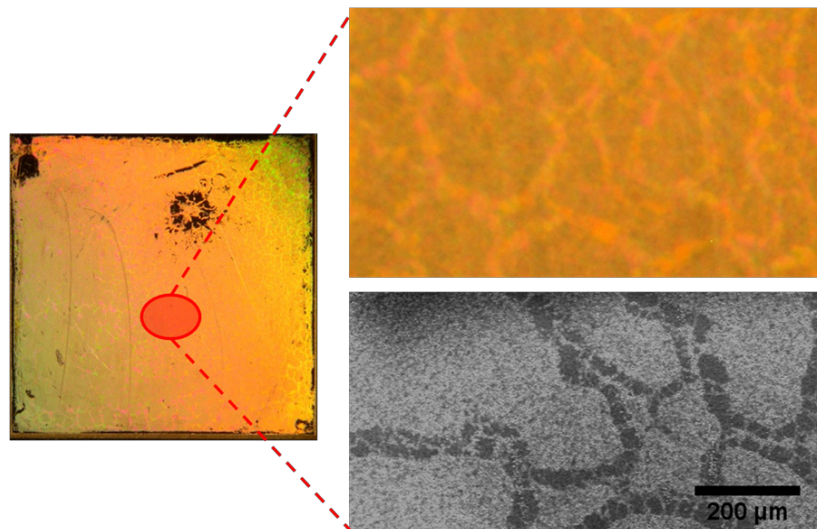
Fig 2.8. Optical and SEM images showing the result of utilizing only one spin coat step in the water-wash method. The darker regions in the SEM image correspond to relatively ordered arrangements of PS beads from the spin coat step; alternatively, the lighter regions correspond to unordered arrangements from the final evaporation step. The substrate shown here is 1 x 1 cm YSZ with gold metal.
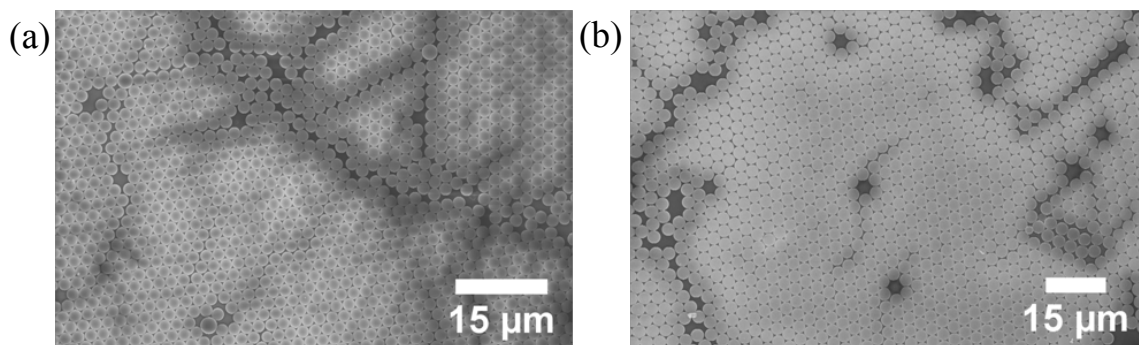
Fig 2.9. Monolayer substrate coverage via multiple spin and wash cycles of polystyrene microspheres on YSZ: (a) 2 μm, and (b) 3.2 μm. Both images contain ~1200 beads.

By this method, it was possible to prepare comprehensive monolayers of PS beads up to 3.2 μm in diameter with the same coverage quality as the nanospheres (compare the nanosphere coverage of Fig. 2.4 to the microsphere coverage of Fig. 2.9). After the microsphere monolayer deposition is complete, the subsequent plasma treatment, metal deposition and template removal steps then proceed as described for the nanosphere lithography, where, again, a minimum of ¼ of the bead diameter must be removed in order to prevent necking during oxygen plasma treatment.

2.3.3   *Microstructural Fidelity*

Given the importance of three-phase boundaries for SOFC electrocatalysis, the 3PB areal density is a key parameter describing the microstructural features of these or any fuel cell electrode. A further important parameter in the case of the two-dimensional electrodes prepared here is the metal coverage, or inversely, the fraction of exposed electrolyte area, i.e., the 2PB areal density. With knowledge of these two parameters and an ability to tune them over a wide range, it becomes possible to achieve the goal of deconvoluting microstructural and compositional influences on electrocatalysis rates.

For a perfect micro-/nanosphere lithographic process in which the template beads display ideal periodicity over the entirety of the substrate, both the 3PB areal density, ρ_{3PB}, and the 2PB area fraction, f_{2PB}, can be computed from knowledge of the starting bead size and the extent of size reduction induced upon plasma etching. The theoretical values of these two quantities are given in equations 2.1 and 2.2, respectively, as functions of the initial (ϕ_i) and final (ϕ_f) diameters of the PS beads.

$$\rho_{3PB}^{theo} = \frac{2\pi}{\sqrt{3}}\left(\frac{\phi_f}{\phi_i}\right)\frac{1}{\phi_i} \qquad (2.1)$$

$$f_{2PB}^{theo} = \frac{\pi}{2\sqrt{3}}\left(\frac{\phi_f}{\phi_i}\right)^2 \qquad (2.2)$$

For an imperfect fabrication process, many kinds of defects exist—disordered regions of PS beads, multilayer and void areas (areal defects); grain boundaries between ordered regions (line defects); and singly missing PS beads within an ordered region (point defects). To assess the influence of these random structural elements, a continuous string of scanning electron microscopy (SEM) images (typically numbering from 100-400 images per sample) was collected from border to border for four representative films. From each image the following parameters were determined: the number and diameter of the pores, the metal|substrate interface length, i.e., 3PB length, and the exposed electrolyte area fraction, i.e., 2PB area fraction. The film characteristics and measured results are summarized below in Table 2.1 and Figures 2.10 and 2.11.

The distribution of pore diameters (Fig. 2.10) in the films was found to be rather narrow, with a Gaussian peak width that is ~ 2% of the mean diameter. This distribution largely reflects the size distribution in the as-purchased PS beads, also about 2%, as oxygen plasma treatment was observed to remove material from the beads in a spatially uniform fashion, both radially and from bead to bead (Fig. 2.1b) [76]. In addition to the
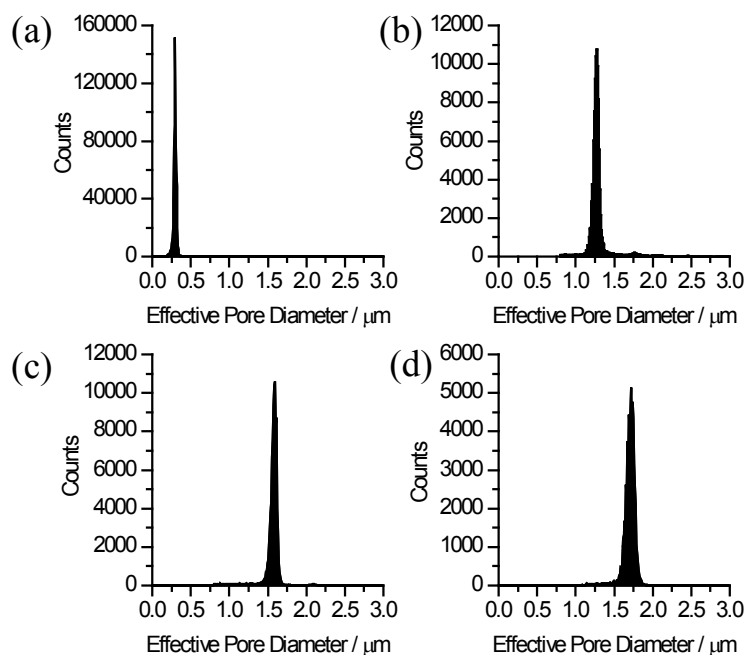
Fig 2.10. Pore diameter histograms of copper networks on YSZ, reflecting the different starting PS bead sizes: (a) 500 nm etched to 300 nm; (b) 2 µm etched to 1.29 µm; (c) 2 µm etched to 1.58 µm; (d) 3.2 µm etched to 1.72 µm.
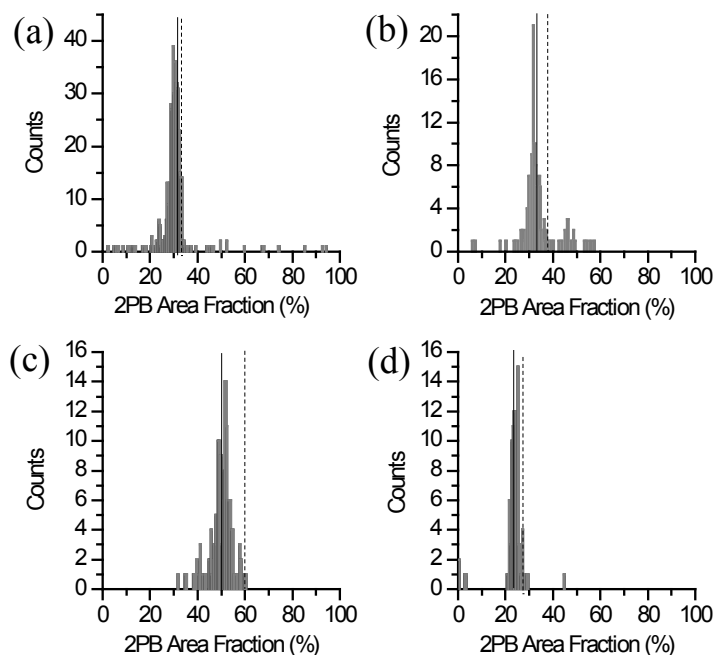
Fig 2.11. 2PB area fraction histograms of copper networks on YSZ, reflecting different starting PS bead sizes: (a) 500 nm etched to 300 nm; (b) 2 µm etched to 1.29 µm; (c) 2 µm etched to 1.58 µm; (d) 3.2 µm etched to 1.72 µm. Solid and dashed lines indicate the average and theoretical values, respectively.

pores represented in the histograms of Figure 2.10, a small number of pores with large

diameters, > 3 μm, was also observed. These are taken to reflect regions in which

multilayers of PS beads occurred, which prevents metal deposition over larger areas (c.f.

Fig. 2.5b). For the PS with an initial diameter of 2 μm, the number of these multilayer-

induced pores is less than 1% of the total; for the 3.2 μm initial diameter spheres, the

number is less than 0.5%; and for the 500 nm spheres, the number is less than 0.1%.

Aside from their statistical insignificance, the contribution of these large diameter pores

to the overall ρ_{3PB} is confirmed to be small, as indicated by the good agreement between

the theoretical and experimental values of this parameter, Table 2.1, and they are omitted

from the plotted range for clarity.

The image-to-image variation in the 2PB area fraction (Fig. 2.11) shows that the

variability in f_{2PB} is more significant than the pore diameter variability. The widest

distribution in f_{2PB} is evident for the film prepared using 500 nm PS beads, where the

standard deviation is 12% of the substrate area (i.e., f_{2PB} is 31.5 ± 12.0%). Moreover, in

all cases, the observed 2PB area was lower than that computed from the initial and final

Table 2.1. Comparison of theoretical and experimental 3PB length areal density and percent 2PB exposure

for different initial PS bead diameters.

Initial bead diameter, ϕ_i/μm	Final pore diameter, ϕ_f/μm	Pore diameter Gaussian width/μm	Theoretical 3PB length density/m cm^{-2}	Experimental 3PB length density/m cm^{-2}	Theoretical percent 2PB exposure	Experimental percent 2PB exposure	2PB exposure standard deviation
0.5	0.3	0.06	435	406	32.6%	31.5%	12.02
2	1.29	0.07	117	112.8	37.7%	33.4%	6.70
2	1.58	0.08	143	137.3	56.6%	49.7%	4.69
3.2	1.72	0.10	61	57.6	26.2%	23.5%	3.60

PS sphere sizes. This can be attributed to the occurrence of point and line defects in the PS two-dimensional crystals, as well as the presence of disordered regions in the monolayer. The statistics surrounding the two films prepared using PS beads with an initial diameter of 2 μm suggest that line and point defects become increasingly important as the extent of etching is minimized. In the case of the film obtained from lightly etched PS beads (ϕ_f = 1.58 μm) there is a large difference between f_{2PB}^{theo} and f_{2PB}^{exp} (56.6 vs. 49.7 %). When the beads are more heavily etched (ϕ_f = 1.29 μm), the difference decreases, whereas the difference between ρ_{3PB}^{theo} and ρ_{3PB}^{exp} and the distribution of pore sizes for the two films are essentially the same. This behavior can be understood as follows. In the case of the lightly etched film, isolated missing beads (both point defects and dislocations behave as isolated, absent beads in a two-dimensional crystal) become a significant portion of the open area available for metal deposition, and, in this manner, such defects increasing in number dominate the coverage features.

The histograms of 2PB area display significant numbers of occurrences outside of what is roughly the main peak. As already indicated, regions with 2PB area below the mean occur as a consequence of defects in the two-dimensional crystals, i.e., voids in the PS bead array, whereas regions with higher fractions of 2PB area occur because multilayers form during the PS bead deposition process, i.e., excessive coverage of the substrate with PS beads. The 500 nm diameter nanospheres generate films in which slightly less than 10% of the regions display significant PS bead void areas, whereas 4% display multi-layered areas. In contrast, for both sizes of microspheres (2 and 3.2 μm) the regions affected by voids in the PS bead array are less than 5%, indicating that the multiple deposition process has more comprehensively filled the monolayer. The

occurrence of multilayer regions for the 2 μm microspheres accounts for 11% of the regions imaged, whereas for the 3.2 μm it is only 1%, suggesting that multi-layer removal becomes facile as the bead size increases.

Overall, despite the imperfection of the monolayer deposition process, the theoretical and experimental values, respectively, of f_{2PB} and of ρ_{3PB} agree quite well with one another, indicating that the fabrication is, in fact, rather controlled. Indeed, all of the experimental ρ_{3PB} values are within 93% of the theoretical, and this was found to hold irrespective of substrate employed or metal deposited. Accordingly, the geometric features of any sample prepared by the methodology presented here can, within a reasonable degree of certainty, be predicted from knowledge of ϕ_i and ϕ_f.

2.3.4 *Thermal Stability*

An additional important characteristic of model fuel cell electrodes is thermal stability. That is, the 3PB length and 2PB area must not change during the course of a high-temperature electrochemical measurement. To evaluate thermal stability, nickel anti-dot networks were annealed at 600 ºC for over 48 hours under humidified hydrogen, typical operating conditions for the anode of an intermediate temperature SOFC. SEM images reveal no discernable microstructural evolution as a consequence of the heat treatment (Fig. 2.12ab), whereas slight changes are visible in the atomic force microscopy (AFM) images (Fig. 2.12cd). Specifically, the nickel surface roughens, from a root mean square roughness of approximately 8 to 14 nm, and the grains undergo slight growth, in a direction limited largely to the surface normal. No other metal networks were subjected to high temperatures.
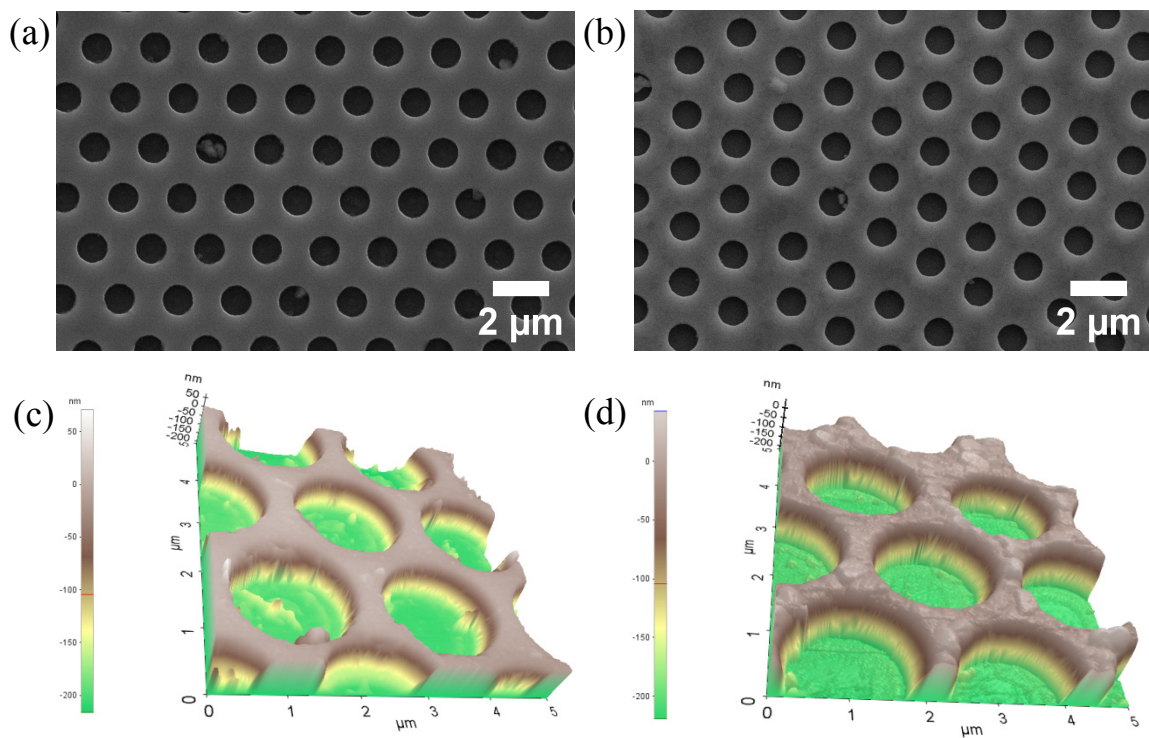
Fig 2.12. Images of an anti-dot porous nickel network (a) and (c) before thermal treatment at 600 ºC under hydrogen (pH$_2$ = 0.1 atm); and (b) and (d) after thermal treatment. (a) and (b) are top-down SEM images; (c) and (d) are AFM images.